Flexible All-Optical 8QAM Signal Format Conversion Using Pump Assisted Nonlinear Optical Loop Mirror

Qiankun Li, Xiongwei Yang, Huashun Wen, Qi Xu, Jiali Yang, Yameng Li, Huajun Yang, Mark S. Leeson *IEEE Senior Member*, Tianhua Xu *IEEE Member*

***Abstract*—A flexible all-optical format interconversion scheme based on a pump assisted nonlinear optical loop mirror (NOLM) is proposed and numerically simulated for the first time to our knowledge. In this scheme, input multi-Gbps 8QAM signals are divided into clockwise (CW) and counter-clockwise (CCW) components by a 3-dB optical coupler (OC), which also couples light from the input pump into the NOLM from the CCW direction. The numerical model of the pump assisted NOLM with CW and CCW optical paths is simplified using a nonlinear Mach-Zehnder interferometer (MZI). Optical signals in the upper MZI arm will be mainly affected by the self-phase modulation (SPM) effect when traversing the highly nonlinear fiber (HNLF) and those in the lower MZI arm are impacted by cross-phase modulation (XPM) in addition to SPM when they experience the HNLF with the input pump light. When the upper-arm optical signal with SPM phase shift and the lower arm optical signal with SPM and XPM phase shifts are coherently mixed, a new converted 8QAM signal can be obtained. The power transfer function (PTF) of the pump assisted NOLM and the relative phase shift (RPS) between the input and the output optical signals are theoretically provided and verified. By only changing the input power of the 8QAM signal and the pump light, all-optical format interconversion of square-, standard- and star-shaped 8QAM signals can be achieved. Furthermore, the proposed scheme can achieve format conversion from the 30 Gbps square-shaped 8QAM signal to a 20 Gbps quadrature phase shift keying (QPSK) signal. The scheme performance is analyzed via constellation diagrams, eye diagrams, the error vector magnitude (EVM) and the bit error rate (BER) of the optical signals. The scheme developed can be deployed in optical gateways to connect different optical networks by dynamically selecting their appropriate modulation formats.**

***Index Terms*—All-optical signal processing, quadrature amplitude modulation, self-phase modulation, cross-phase modulation, nonlinear optical loop mirror.**

Manuscript received March 03, 2023; revised May 12, 2023; accepted June 15, 2023. (*Corresponding author: Huashun Wen, Huajun Yang and Tianhua Xu.*)

This work was supported by National Key R&D Program of China under grants 2019YFB2203104 and 2020YFB2205801 and by National Natural Science Foundation of China under grant 11574042 and by EU Horizon 2020 MSCA Grant 101008280 (DIOR) and UK Royal Society Grant (IES\R3\223068).

Q. Li and H. Yang are with School of Physics, University of Electronic Science and Technology of China, Chengdu 610054, China. X. Yang is with School of Information and Technology, Fudan University, Shanghai 200433, China. H. Wen is with the State Key Laboratory on Integrated Optoelectronics, Institute of Semiconductors, Chinese Academy Sciences, Beijing 100083, China and the School of Electronic, Electrical and Communication Engineering, University of Chinese Academy of Sciences, Beijing 100049, China. Q. Xu is with school of information and electronics, Beijing Institute of Technology, Beijing 100081, China. J. Yang is with School of Information and Communication Engineering, Beijing University of Posts and Telecommunications, Beijing 100876, China. Y. Li is with School of Environment, Tsinghua University, Beijing 10084, China. M. S. Leeson is with School of Engineering, University of Warwick, Coventry CV4 7AL, United Kingdom. T. Xu is with School of Engineering, University of Warwick, Coventry CV4 7AL, United Kingdom, with Tianjin University, Tianjin 300072, China, and also with University College London (UCL), London WC1E 6BT, United Kingdom. (e-mail: liqk@bupt.cn; yanghj@uestc.edu.cn; xwyang22@m.fudan.edu.cn; whs@semi.ac.cn; 3220215105@bit.edu.cn; yangjiali@bupt.edu.cn; lymx-in@126.com; mark.leeson@warwick.ac.uk; Tianhua.Xu@warwick.ac.uk).

I. Introduction

With the development and application of the fifth-generation (5G) and sixth generation (6G) mobile communication technologies, the Internet of Things (IoT), the Internet of Energy (IoE), automatic driving (AD), ultra-high definition (UHD) video streams, various types of data traffic are facing explosive growth of data rates in optical networks [1]–[4]. According to Cisco, compound annual growth rates (CAGRs) from 2018 to 2023 for global Internet users have been 6% and for mobile devices and connection have been 8% [5]. Whilst more and more large-bandwidth and low-latency services put forward stricter requirements for optical network nodes, homogeneous and heterogeneous optical networks are also required to be all-optically interconnected via optical network nodes. Thus, to transmit data traffic across such optical networks, flexible and re-configurable optical network nodes able to optically interconnect diverse optical networks with different modulation formats become very important. All-optical signal processing (AOSP) provides an effective method for flexible all-optical networks (AONs), since processing photons offers, inter alia, large-bandwidth, low-latency and parallel processing [6]. Generally, data transmission between different optical network variants will be via optical nodes, connecting for instance, backbone optical networks (BONs) to metro access networks (MANs) or local access networks (LANs). These optical networks usually differ in their data traffic types, network dimensions, access terminals and so on, with corresponding optimal modulation formats for each [7], [8]. Advanced modulation formats including m-ary quadrature amplitude modulation (mQAM) and m-ary phase shift keying (mPSK) have higher spectrum efficiency (SE) and better chromatic dispersion (CD) tolerance. Typical examples are 8QAM, 8PSK and 16QAM [8]–[11], which have been investigated and implemented in a range of optical networks [12]–[15]. Optical nodes must perform format conversion to ensure effective data transmission between optical networks with different optimal modulation formats. This has resulted in all-optical format conversion (AOFC) technology based on ultra-fast nonlinear effects in a variety of nonlinear media becoming an important research focus in flexible AONs [16]–[20].

Lightwaves clearly possess multiple physical characteristics that can be modulated to convey information and converting between the various modulation dimensions and formats requires different format conversion approaches, for example from phase to intensity. Aggregation and de-aggregation between low-order and high-order modulation formats for many modulation formats have been investigated widely to connect different LANs and BONs [4], [18], [21]. Aggregating simple modulation formats into an advanced modulation format improves SE, for example when simply modulated data traffic for the same destination originates from different LAN users, the branch data traffic can be aggregated to form traffic employing advanced modulation formats. De-aggregation can be applied when traffic using advanced modulation formats comes from a BON with different user destinations to recover the simple modulation formats. This allows the use of simpler and cheaper LAN receivers, since individual users often do not require all the data from an advanced modulation format [22]. Although aggregation and de-aggregation between low-order and high-order modulation formats are key technologies in flexible AONs, another key to information transmission between optical networks with different modulation formats is conversion without changing the modulation order [6]. For example, the all-optical conversion of QPSK and PAM4 signals or standard-shaped 8QAM (standard-8QAM), square-shaped 8QAM (square-8QAM) and 8PSK signals [23]–[26]. The conversion of format produces no information loss or information redundancy and is thus extremely important in future AON implementation.

However, in the schemes referenced above, modulation format interconversion was implemented based on discrete design schemes, requiring the deployment of at least two sets of independent devices, increasing optical node complexity and construction cost.

8QAM has better tolerance to the noise than 16QAM signals and higher information capacity than QPSK [3], [9], meaning that it has been widely implemented in 100 Gbps optical transmission systems and beyond [27]–[30]. The transmission performance of different 8QAM signals in a variety of optical transmission systems has also been investigated and compared [31]–[36]. AOFC of different 8QAM signals will be needed at optical network nodes when they are selected in different optical transmission systems. For example, when the information loaded on standard-8QAM are transmitted from fixed optical networks to free-space optical networks or visible light communication (VLC) optical networks loaded on square-8QAM, the format conversion is needed to be performed at optical network nodes [30], [33], [37]. Format conversion of star-8QAM to standard-8QAM using phase-sensitive amplification (PSA) has been reported to connect different optical networks [38]. The same method has also been employed to convert square-8QAM to standard-8QAM with regeneration [25]. However, these schemes required phase-matching conditions to ensure effective four-wave mixing (FWM) and did not demonstrate the inverse optical format

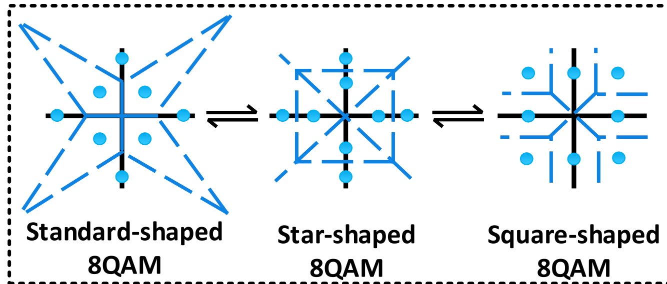

Fig. 1. Constellations of standard-, star- and square-shaped 8QAM signals.

conversion process. Another approach has been to utilize a nonlinear Mach-Zehnder interferometer (MZI) for conversion from standard-8QAM signals to square-8QAM signals [26]. However, experimental implementation was prone to temperature drift, vibration and other volatile environmental factors.

To the best of our knowledge, there has been no effective scheme to achieve the all-optical format interconversion between star-8QAM, square-8QAM and standard-8QAM (with constellation diagrams as shown in Fig. 1) within a single format conversion device. In this paper, a flexible all-optical format interconversion scheme between the 8QAM variants based on a pump assisted nonlinear optical loop mirror (NOLM) is proposed for the first time and numerically evaluated. This all-optical format interconversion method is able to increase optical node utility in the AOSP and promote the flexible interconnection of different optical networks. Moreover, the scheme also improves the utilization efficiency of the optical conversion equipment and a pump assisted NOLM has better environmental stability than a nonlinear MZI. An input 10 GBaud star-8QAM signal can be converted into a 10 GBaud square-8QAM signal or a 10 GBaud standard-8QAM signal by adjusting the input power of the star-8QAM signal and the pump level. The same pump assisted NOLM can also convert an input 10 GBaud standard-8QAM signal into a 10 GBaud star-8QAM signal or an input 10 GBaud square-8QAM signal into a 10 GBaud star-8QAM signal. The star-8QAM signal can be considered as the intermediate optical signal in the all-optical format interconversion of the rectangular-8QAM signal and the standard-8QAM signal, as shown in Fig. 1. The constellation diagrams may be used to demonstrate the efficacy of the proposed all-optical format interconversion for star-, rectangular- and standard-8QAM signals. The error vector magnitude (EVM) and the bit error rate (BER) of the relative optical signals before and after the interconversion may be determined to evaluate the scheme performance. Moreover, 30 Gbps square-8QAM can also be converted into 20 Gbps QPSK just by varying the power of the input pump.

II. Theory and Operation Principle

A schematic diagram of the pump assisted NOLM is shown in Fig. 2(a). Since the NOLM structure was proposed for the first time in 1988 [39], it has been widely investigated in ultra-fast optical signal processing, for example in amplitude regeneration, multiplexing and demultiplexing, analog-to-digital conversion (ADC), millimeter wave generation and format

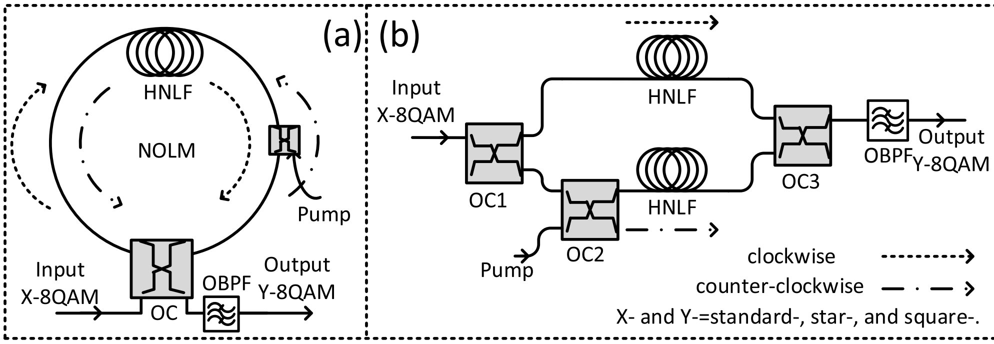

Fig. 2. Schematics of (a) the proposed pump assisted NOLM and (b) the corresponding simplified nonlinear MZI model.

conversion [18], [40]–[45]. Its inherent symmetric structure in two arms enables the clockwise (CW) optical pulses and the counter-clockwise (CCW) optical pulses to experience the same time delay. When these CW and CCW pulses have the same input power, the nonlinear phase shifts generated by self-phase modulation (SPM) both pulses are the same. The pump assisted NOLM designed here is formed by introducing an additional pump beam into the CCW arm. The cross-phase modulation (XPM) phase shift produced by this CCW pump is added to the transmitted CCW optical pulse. The nonlinear phase difference between the CW and the CCW optical paths is very important in the NOLM, which can be usually used to realize various optical signal processing functions, including adjustment of the amplitude and the phase distributions of the input optical signals. Moreover, marginal and undesired counterpropagating nonlinear effects, such as polarization mode dispersion (PMD), stimulated Raman scattering (SRS) and stimulated Brillouin scattering (SBS) can be neglected in the simulation scheme. XPM phase shifts generated by the CW and the CCW signals on the counterpropagating optical pulses are constant and marginal and can also be neglected [41], [46], [47]. At this time, the proposed pump assisted NOLM structure with the CW and the CCW optical paths in Fig. 2(a), can be simplified into an equivalent nonlinear MZI model with upper and lower arms shown in Fig. 2(b).

As illustrated in Fig. 2(b), the input optical signal is split equally by the first 3-dB optical coupler (OC1). The pump and the signal in the lower arm are mixed in OC2 and the resultant signal fed into the lower arm highly nonlinear fiber (HNLF). The input optical signal in the upper arm is also fed into the same HNLF. Finally, the outputs of the upper and lower arms are mixed in OC3. An optical band-pass filter (OBPF) with the same center frequency as input is used to filter out the converted optical signal. Only the nonlinear phase shift introduced by SPM is added to the upper arm signal that enters the HNLF, whereas when that from the lower arm enters the same HNLF with the pump, the XPM-induced nonlinear phase shift is added to the signal in addition to the effect of SPM. Thus, the coherent addition of the upper arm signal (with SPM only) to the lower arm signal (with SPM and XPM) enables flexible change of the amplitude and phase of the original optical input signal. The optical output signal phase and the amplitude distributions depend on the nonlinear phase shift difference between the signals in the two arms [19]. When XPM occurs, power will flow between the input signal and the pump, known as parametric amplification (PA). We now present the mathematical analysis of the interaction between the signal and the pump in the HNLF, based on the nonlinear Schrödinger equation.

The mathematical relationship between the input and the output ports of the 3-dB OC can be written as:

$$\begin{pmatrix} E_{1,out} \\ E_{2,out} \end{pmatrix} = \frac{\sqrt{2}}{2} \begin{pmatrix} 1 & i \\ i & 1 \end{pmatrix} \cdot \begin{pmatrix} E_{1,in} \\ E_{2,in} \end{pmatrix} \tag{1}$$

$E_{1,in}$, $E_{2,in}$ represent the electric fields of the input optical signals, respectively. $E_{1,out}$, $E_{2,out}$ represent the electric fields of the output optical signals, respectively. In the proposed pump assisted NOLM configuration, there is only one input 8QAM signal (of square, standard or star format), which can be represented by $E_{1,in}$, so $E_{2,in}$ is zero. For OC1, the output for the upper arm optical signal can be expressed as:

$$E_{1,out} = \frac{\sqrt{2}}{2} E_{1,in} \tag{2}$$

The output of the lower arm optical signal can be written as:

$$E_{2,out} = i\frac{\sqrt{2}}{2} E_{1,in} \tag{3}$$

Without considering the optical frequency oscillation item, the electrical field of the input 8QAM signal can be written as:

$$E_{1,in} = A_{in} \cdot e^{i\varphi_{in}} \tag{4}$$

A_{in} and φ_{in} represent the amplitude and the initial phase of the input optical signal; the initial phase of the pump is zero. Assuming that the input signal and input pump have the same polarization states, e. g., x-polarization. Moreover, the polarization controller (PC) is used to ensure the polarization states of the input signal and the input pump light to be alignment in the practical experiment. For OC2, the output electrical field from its bar port can be expressed as:

$$\begin{aligned} E^1_{oc2} &= \frac{\sqrt{2}}{2} E_{2,out} + \frac{\sqrt{2}}{2} i E_{pump} \\ &= \frac{1}{2} i A_{in} e^{i\varphi_{in}} + \frac{\sqrt{2}}{2} i A_{pump} e^{i\varphi_{pump}} \\ &= \frac{1}{2}\sqrt{P_{in}} e^{i(\varphi_{in}+\frac{\pi}{2})} + \sqrt{\frac{P_{pump}}{2}} e^{i\frac{\pi}{2}} \end{aligned} \tag{5}$$

E^1_{oc2} represents the electric field of the output lightwaves from the through port of OC2. E_{pump} represents the electric filed of the input pump light. A_{pump} and φ_{pump} represent the amplitude and the initial phase of the pump; P_{in} and P_{pump} are the input powers of the input and pump signals, respectively. Thus, when the lower arm input and the pump are mixed at OC2, the output optical signal and output pump from the through port of OC2 are fed into the HNLF. At this time, the first term and the second term in Equation (5) can be considered as the new input signal and pump for the next loop iteration.

Namely, when the signal and the pump are coupled into the HNLF, their electric fields can be rewritten as:

$$\begin{cases} E_s = \frac{1}{2}\sqrt{P_{in}} e^{i(\varphi_{in}+\frac{\pi}{2})} = \frac{1}{2}\sqrt{P_{in}} e^{i\varphi_1} \\ E_{pump} = \sqrt{\frac{P_{pump}}{2}} e^{i\frac{\pi}{2}} = \sqrt{\frac{P_{pump}}{2}} e^{i\varphi_0} \end{cases} \tag{6}$$

Then, the amplitude and the phase of the new input signal are $\frac{1}{2}\sqrt{P_{in}}$ and φ_1, respectively. The amplitude and the initial phase of the new input pump are $\sqrt{\frac{P_{pump}}{2}}$ and φ_0, respectively. When the optical signal and the pump light are coupled into the HNLF, harmonics will be generated due to the FWM effect. The electric fields of the harmonics can be written as [48]:

$$\begin{aligned} &\sqrt{P'_m} e^{i(\omega'_m t+\varphi'_m)} \\ =&[i^m \sqrt{P_0} J_m(2\gamma L\sqrt{P_0P_1}) + i^{m-1}\sqrt{P_1} J_{m-1}(2\gamma L\sqrt{P_0P_1})] \\ &\cdot e^{i\gamma P_0 L} \cdot e^{i\gamma P_1 L} \cdot e^{i[m(\omega_1 t+\varphi_1)-(m-1)(\omega_0 t+\varphi_0)]} \end{aligned} \tag{7}$$

Take an integer for m. ω'_m represent the angular frequencies of harmonics. When $m = 1$, the output harmonic is just the output optical signal. ω'_1 and ω_1 represent the angular frequencies of the output and input optical signals. Thus, ω'_1=ω_1. ω_0 represents the angular frequency of the input pump light. The electric field of the output signal satisfies the following expression [48]:

$$\begin{aligned} &\sqrt{P'_1} e^{i(\omega'_1 t+\varphi'_1)} \\ =&[i\sqrt{P_0} J_1(2\gamma L\sqrt{P_0P_1}) + \sqrt{P_1} J_0(2\gamma L\sqrt{P_0P_1})] \\ &\cdot e^{i\gamma P_0 L} \cdot e^{i\gamma P_1 L} \cdot e^{i(\omega_1 t+\varphi_1)} \\ =&\sqrt{P_0 J_1^2(2\gamma L\sqrt{P_0P_1}) + P_1 J_0^2(2\gamma L\sqrt{P_0P_1})} \\ &\cdot e^{i(\omega_1 t+\varphi_1+\gamma P_0 L+\gamma P_1 L)} \cdot e^{i\varphi_{bom}} \\ =&Ae^{i(\omega_1 t+\varphi_A)} \end{aligned} \tag{8}$$

where

$$\begin{cases} \varphi_{bom} = arctan\frac{\sqrt{P_0}J_1(2\gamma L\sqrt{P_0P_1})}{\sqrt{P_1}J_0(2\gamma L\sqrt{P_0P_1})} \\ \varphi_A = \varphi_1 + \gamma P_0 L + \gamma P_1 L + \varphi_{bom} \\ A^2 = P_0 J_1^2(2\gamma L\sqrt{P_0P_1}) + P_1 J_0^2(2\gamma L\sqrt{P_0P_1}) \end{cases} \tag{9}$$

P_0 and P_1 represent the power of the input optical signal and the pump light, respectively. J_0 and J_1 represent the Bessel functions, respectively. γ and L represent the nonlinear coefficient and the effective HNLF length, respectively. Notably, By use of (6), φ_1, P_1, P_0 in (7), (8) and (9) can be expressed as:

$$\begin{cases} \varphi_1 = \varphi_{in} + \frac{\pi}{2} \\ P_1 = \frac{1}{4}P_{in} \\ P_0 = \frac{1}{2}P_{pump} \end{cases} \tag{10}$$

Thus, the output optical signal from the lower arm HNLF can be rewritten as:

$$E^{low}_{3,in} = A \cdot e^{i\varphi_A} \tag{11}$$

The upper arm output signal is affected only by SPM when it traverses the upper arm HNLF. Its optical field can be expressed as:

$$\begin{aligned} E^{up}_{3,in} &= \sqrt{\frac{P_{in}}{2}} e^{i(\varphi_{in}+\varphi_{spm})} \\ &= \sqrt{\frac{P_{in}}{2}} e^{i(\varphi_{in}+\frac{\gamma L P_{in}}{2})} \end{aligned} \tag{12}$$

Finally, at OC3, the through signal can be written as:

$$\begin{aligned} E^{up}_{3,out} &= \frac{\sqrt{2}}{2}E^{up}_{3,in} + i\frac{\sqrt{2}}{2}E^{low}_{3,in} \\ &= \frac{\sqrt{P_{in}}}{2} e^{i(\varphi_{in}+\frac{\gamma L P_{in}}{2})} + \frac{A}{\sqrt{2}} e^{i(\varphi_A+\frac{\pi}{2})} \\ &= Me^{i\varphi_M}\cdot e^{i\varphi_{in}} + Ne^{i\varphi_N}\cdot e^{i\varphi_{in}} \\ &= A_{out}\cdot e^{i\varphi_{out}} \end{aligned} \tag{13}$$

The transmission coefficient (TC) is defined as the ratio between the output and input optical signals:

$$TC = \frac{E^{up}_{3,out}}{E_{1,in}} = \frac{A_{out}e^{i\varphi_{out}}}{A_{in}e^{i\varphi_{in}}} = \frac{A_{out}}{A_{in}}e^{i\varphi_{rps}} \tag{14}$$

From (13) and (14), the output power transfer function (PTF) and the relative phase shift (RPS) can be expressed as:

$$\begin{cases} P_{out} = M^2 + N^2 + 2MNcos(\varphi_M - \varphi_N) \\ \varphi_{rps} = \varphi_{out} - \varphi_{in} = arctan\frac{Msin\varphi_M + Nsin\varphi_N}{Mcos\varphi_M + Ncos\varphi_N} \end{cases} \tag{15}$$

where

$$\begin{cases} M = \frac{\sqrt{P_{in}}}{2} \\ N = \frac{A}{\sqrt{2}} \\ \varphi_M = \frac{1}{2}\gamma L P_{in} \\ \varphi_N = \varphi_{bom} + \frac{1}{4}\gamma L P_{in} + \frac{1}{2}\gamma L P_{pump} + \pi \end{cases} \tag{16}$$

To observe the PTF and the RPS of the pump assisted NOLM, square-8QAM was first applied to verify the format conversion from this to star-8QAM. In the test, the HNLF considered had a nonlinear coefficient of 13.1 (km·W)$^{-1}$, an effective length of ∼550 m and a dispersion parameter of 1.6×10^{-6} s/m^2; the reference frequency was 193.1 THz and fiber losses were neglected. The input square-8QAM had a frequency of 193.1 THz at average power of 24 dBm. The input pump light had a frequency of 193.07 THz at average power of 10 dBm (P_{pump}=10 dBm). The modulation index (MI) of the inner and the outer rings of the square-8QAM was 0.5. The MI is defined as the ratio of the difference in power between the outer ring and the inner ring constellations

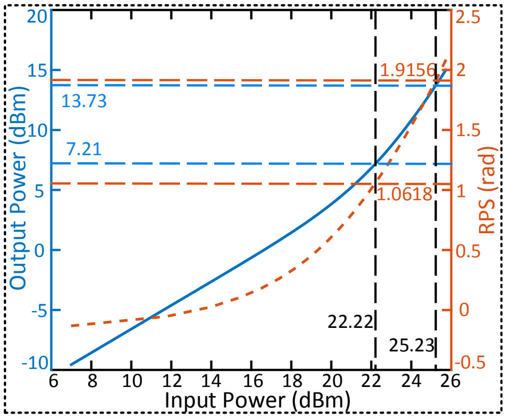

Fig. 3. PTF and RPS versus the input power for the format conversion from the square-shaped 8QAM signal to the star-shaped 8QAM signal.

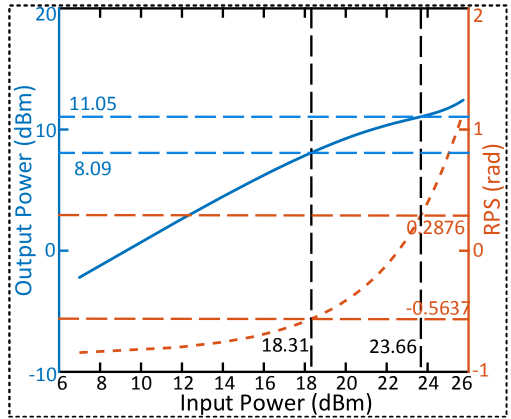

Fig. 4. PTF and RPS versus the input power for the format conversion from the star-shaped 8QAM signal to the square-shaped 8QAM signal.

to the power of the outer ring constellations. The mathematical expression can be written as:

$$MI = \frac{P_{outer} - P_{inner}}{P_{outer}} \quad (17)$$

P_{inner} and P_{outer} represent the inner and outer rings power of the input 8QAM signal. The PTF and the RPS as functions of the power of the input optical signal are shown in Fig. 3. Since the powers of the inner and outer rings of the input square-8QAM are 22.22 dBm and 25.23 dBm, respectively, the corresponding output powers are ∼7.21 dBm and ∼13.73 dBm. The corresponding RPS values of the inner and the outer rings are ∼1.0618 rad and ∼1.9156 rad, respectively. Although the output optical signal still has two inner and the outer ring intensity level, the phase difference between the two corresponding RPSs is ∼0.85 rad, i.e., ∼48.9°. This can be utilized to compensate for the phase offset of 45° between the inner and the outer rings of the input square-8QAM signal, leaving a residual difference in the output 8QAM signal of just 3.9°. Clearly, this is much less than the input square-8QAM signal 45° phase difference and an acceptably small error. In addition, considering that the nonlinear phase shift introduced by the outer ring constellation points is higher than that introduced by the inner ring constellation points, the 3.9° phase difference between the inner and the outer rings in the output 8QAM signal can also be neglected. Namely, the output 8QAM signal can be deemed star-8QAM and the input square-8QAM has been converted into star-8QAM.

We also verified the format conversion from a star-8QAM signal to a square-8QAM signal with the same HNLF parameters. The input signal was a 21.8 dBm (average power) star-shaped 8QAM signal with a MI of 0.708 and the input pump power was 20.4 dBm. The PTF and the RPS functions with the input power were determined and are shown in Fig. 4. Since the input inner and outer rings of the star-shaped 8QAM signal had powers of 18.31 dBm and 23.66 dBm, respectively, the corresponding output powers were 8.09 dBm and 11.05 dBm. The power gap between the output inner and outer rings was 2.96 dB, close to the ideal square-8QAM value of 3 dB. The inner and the outer rings of star-8QAM are in phase but ideal square-8QAM has a phase difference of 45° between

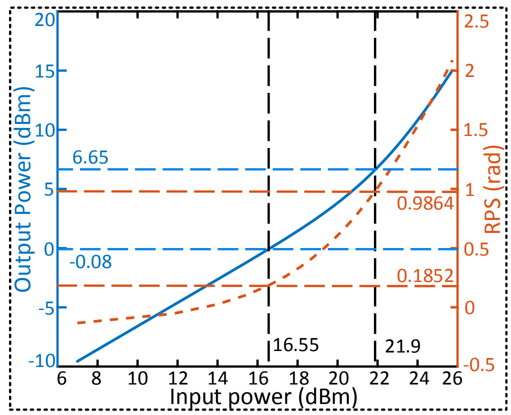

Fig. 5. PTF and RPS versus the input power for the interconversion between star-shaped 8QAM and standard-shaped 8QAM.

the inner and the outer rings. For the input star-8QAM, the corresponding output RPSs of the inner and the outer rings were -0.5637 rad and 0.2876 rad, respectively. Thus, there is a phase difference gap of ∼48.8°, which is again close to 45°. Considering that the nonlinear phase shift introduced by the inner and the outer rings of the input star-8QAM signal is different, the extra phase difference of 3.8° in the RPS can also be accepted for the converted square-8QAM signal. Therefore, conversion of star-8QAM into square-8QAM can be achieved based on the same pump assisted NOLM configuration by changing the signal and pump input power.

For standard-8QAM to star-8QAM conversion, we consider a standard-8QAM signal with a MI of 0.708 and 20 dBm average input power, with corresponding inner and outer ring powers of 16.55 dBm and 21.9 dBm, respectively. Using a 10 dBm pump, the PTF and the RPS functions with the input optical signal power are shown in Fig. 5. The corresponding output powers of the rings in the optical signal were -0.08 dBm and 6.65 dBm, respectively. So, the output optical signal still has two intensity levels with corresponding RPSs of ∼0.1852 rad and ∼0.9864 rad, respectively; i.e. a gap of ∼0.8 rad or ∼45.84°. This can also be used to compensate for the inherent phase offset of 45° between the inner and the outer rings in the input standard-8QAM with an error of ∼2%. Thus, the

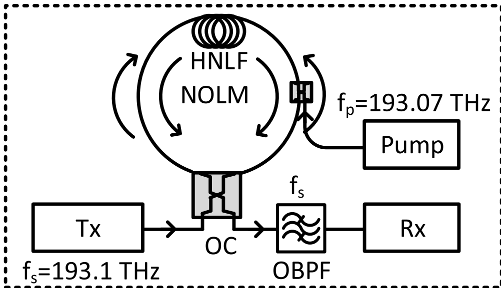

Fig. 6. The proposed scheme of all-optical format interconversion, Tx: Transmitter, Rx: Receiver.

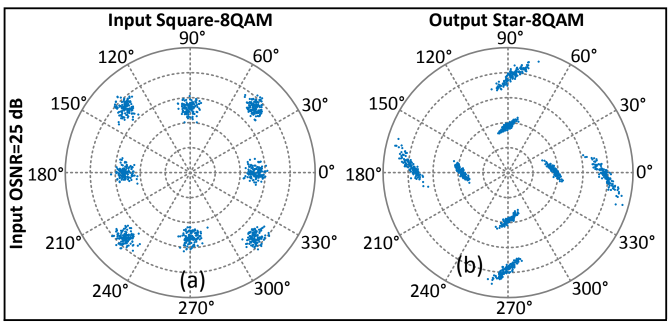

Fig. 7. Constellations of (a) the input 30 Gbit/s square-shaped 8QAM signal, (b) the output star-shaped 8QAM signal.

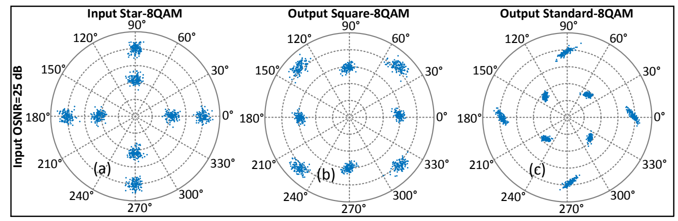

Fig. 8. Constellations of (a) the input 30 Gbit/s star-shaped 8QAM signal, (b) the output square-shaped 8QAM signal and (c) the output standard-shaped 8QAM signal.

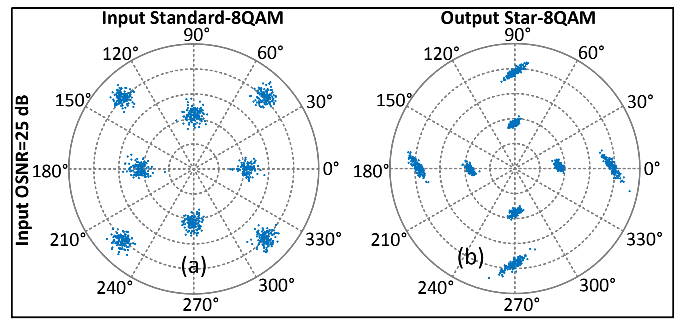

Fig. 9. Constellations of (a) the input 30 Gbit/s standard-shaped 8QAM signal, (b) the output star-shaped 8QAM signal.

result was successfully conversion to star-8QAM.

Similarly, when a 20 dBm (average power), 0.708 MI star-8QAM was injected into the pump assisted NOLM, with the same physical parameters, its corresponding PTF and RPS functions were as presented in Fig. 5. The input star-shaped 8QAM signal had no phase difference between its inner and outer rings but a phase difference 45.84° was generated with the same 2% error observed for conversion the in the other direction. The output signal preserved two inner and the outer ring intensity levels, as shown in Fig. 5. Therefore, input star-8QAM was successfully converted into standard-8QAM based on the same pump assisted NOLM.

Above all, for each type of format conversion, both PTF and RPS can be obtained through equations (15) and (16). TABLE I shows the input and output power and RPSs of optical signals and pump lights before and after format conversion. The format conversion processing for different input 8QAM signals can be seen more clearly.

III. Simulations and Discussions

The proposed all-optical format interconversion configuration is shown in Fig. 6. A configurable optical transmitter was used to generate the input 10 GBaud square-, standard-, and star-shaped 8QAM signals at a center frequency of 193.1 THz. In the simulation, the transmitter comprised a cascaded phase modulator (PM) and amplitude modulator (AM), a pseudo-random binary sequence (PRBS) generator, non-return zero (NRZ) coders and a laser (the linewidth of which was neglected). An amplified spontaneous emission (ASE) noise source was used to change the input optical signal-to-noise ratio (OSNR) followed by an OBPF to remove the out-of-band noise. An OC was used to separate the various input 8QAM signals into upper arm and the lower arm optical signals. A 193.07 THz pump was coupled into the pump assisted NOLM from the lower arm direction. Notably, in the practical optical transmission systems, the polarization states of the signal and the pump need to be alignment by the PC. The SBS threshold of the HNLF used also need to be increased by applying a temperature distribution, applying a strain gradient, pre-processing by the phase modulation or other promising methods [49]–[51]. When optical signals in the upper arm and the lower arm passed through the HNLF, they were coherently superposed in the OC. An OBPF centered on 193.1 THz was placed after the through port of the OC to filter out the converted 8QAM signal. Finally, the output optical signal was demodulated by the coherent receiver. The HNLF used in the pump assisted NOLM had the same physical parameters as those in Section II and a dispersion slope of 0.02 ps/((nm)^{2}km). When a 24 dBm (average power) input square-8QAM signal and 10 dBm pump were injected into the pump assisted NOLM, a converted star-8QAM signal was obtained, as shown in Fig. 7. When a 21.8 dBm (average power) input star-8QAM signal (Fig. 8(a)) and 20.4 dBm pump were applied, a converted square-8QAM signal was extracted, as shown in Fig. 8(b). Similarly, when the input was star-8QAM signal with an input average power of 20 dBm using a pump of 10 dBm, a converted standard-8QAM signal was generated, as shown in Fig. 8(c). When an input average power of 20 dBm standard-8QAM signal and 10 dBm pump were applied, a converted star-8QAM signal was produced, as shown in Fig. 9.

To characterize the degree of noise interference on the

TABLE I
POWER AND RPSS RELATIONSHIPS OF INPUT AND OUTPUT OPTICAL SIGNALS BEFORE AND AFTER FORMAT CONVERSION.

Input signal	signal Average power	Input inner ring	Input outer ring	Pump power	Output inner ring	Output outer ring	RPS of inner ring	RPS of outer ring	Output signal
Square-8QAM	24 dBm	22.22 dBm	25.23 dBm	10 dBm	7.21 dBm	13.73 dBm	1.0618 rad	1.9156 rad	Star-8QAM
Star-8QAM	21.8 dBm	18.31 dBm	23.66 dBm	20.4 dBm	8.09 dBm	11.05 dBm	-0.5637 rad	0.2876 rad	Square-8QAM
Standard-8QAM	20 dBm	16.55 dBm	21.90 dBm	10 dBm	-0.08 dBm	6.65 dBm	0.1852 rad	0.9864 rad	Star-8QAM
Star-8QAM	20 dBm	16.55 dBm	21.90 dBm	10 dBm	-0.08 dBm	6.65 dBm	0.1852 rad	0.9864 rad	Standard-8QAM

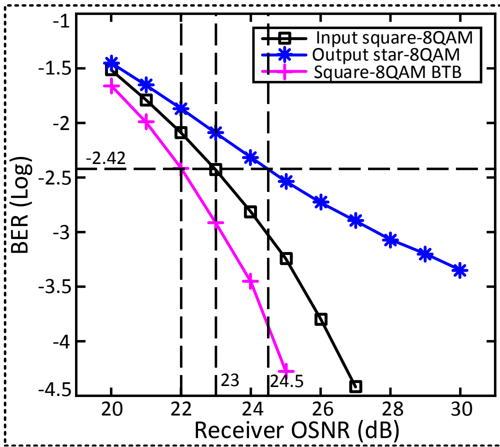

Fig. 10. BER versus receiver OSNR for the format conversion of square-shaped 8QAM to star-shaped 8QAM with the input OSNR of 25 dB.

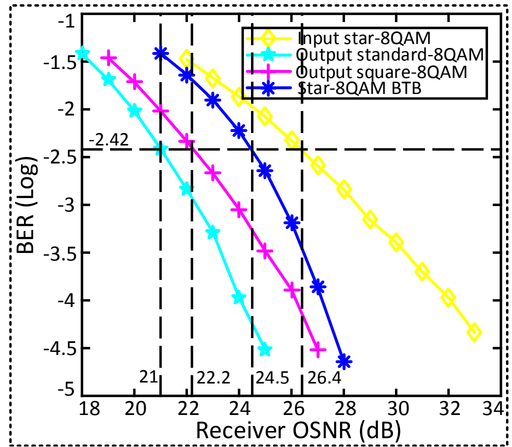

Fig. 11. BER versus receiver OSNR for the format conversion of star-shaped 8QAM to standard-shaped 8QAM and square-shaped 8QAM with the input OSNR of 25 dB.

optical signal in the transmission process, an ASE noise source was added to change the receiver OSNR. A sequence of 2^{17} signal symbols was applied to calculate the BER performance of the input and the output optical signals when the receiver OSNR varied for an input OSNR of 25 dB. Fig. 10 shows the BER performance for the conversion from square-8QAM to star-8QAM before and after the pump assisted NOLM. The corresponding EVM values were 8.89% for the input square-8QAM and 11.37% for the converted star-8QAM. OSNR values of 22 dB, 23 dB and 24.5 dB were required achieve a hard-decision forward-error-correction (HD-FEC) threshold of 3.8×10^{-3} (log value of -2.42), for ideal square-8QAM with back-to-back (BTB) transmission, input square-8QAM and output star-8QAM, respectively. There was thus a power penalty of 1.5 dB resulting from the format conversion. It can be seen from the constellations in Fig. 7 that significant nonlinear phase noise induced by the SPM and XPM effects was added to the output star-8QAM. The power ratio (PR) between the inner and the outer rings of the star-8QAM signal has a significant impact on its BER performance, which is also impacted by the phase distance (PD) and the amplitude distance (AD) of the adjacent constellations [19]. The generated nonlinear phase noise makes the PD shorter, which leads to the degradation of the phase noise tolerance in the converted star-8QAM signal. Although the nonlinear phase noise induced by SPM and XPM effects can degrade the phase noise tolerance of star-8QAM, optical nonlinear regenerators can be deployed to mitigate this negative impact [51], [52].

Fig. 11 shows the BER performance versus the receiver OSNR for conversion from a star-8QAM input to standard-8QAM and the square-8QAM. At the HD-FEC threshold, the corresponding receiver OSNRs are 26.4 dB, 21 dB and 22.2 dB, respectively. Clearly, compared to the input star-8QAM, the converted standard- and square-8QAM signals offer OSNR advantages of 4.2 dB and 5.4 dB, respectively. Moreover, there is a 1.2 dB OSNR advantage in favor of standard-8QAM over square-8QAM in the output signals. For the ideal star-8QAM signal with BTB transmission, the corresponding receiver OSNR is 24.5 dB. the converted standard- and square-8QAM signals also offer OSNR advantages of 3.5 dB and 2.3 dB. In the proposed scheme, the star-8QAM generated has a larger PR, which makes it more easily distorted by amplitude noise, as shown in Fig. 8(a). For the converted standard- and square-8QAM signals, the constellation points of the inner and the outer rings of both signals have a phase offset of approximately 45°, as shown in Fig. 8(b)-(c), allowing the converted optical signals to achieve a better balance in tolerating amplitude and phase noise. The smallest Euclidian distance between adjacent constellation points in standard-8QAM is larger than that in square-8QAM, meaning it usually has a better noise tolerance, which translates to the superior BER performance seen in Fig. 11. For an input OSNR of 25 dB, the EVMs of the input star-8QAM signal and the output standard- and square-8QAM signals were 9.18%, 7.49% and 8.52%, respectively. Thus, the standard- and square-8QAM outputs showed respective improvements of 1.69% and 0.66%. Therefore, format conversion from star-8QAM to standard- and square-shaped 8QAM also offers all-optical regeneration with geometric constellation shaping (GCS).

Fig. 12 shows the BER performance versus receiver OSNR for conversion from standard-8QAM to star-8QAM. At an

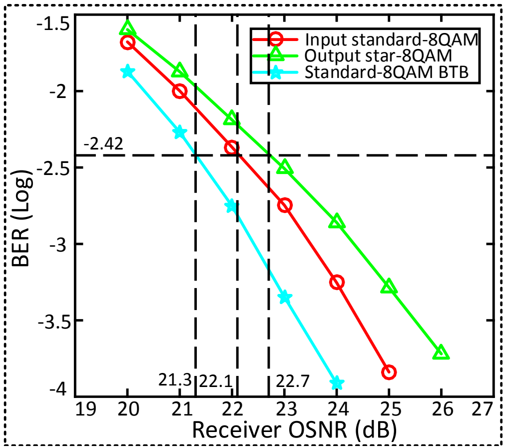

Fig. 12. BER versus receiver OSNR for the format conversion of standard-shaped 8QAM to star-shaped 8QAM with the input OSNR of 25 dB.

input OSNR of 25 dB, the input and output EVMs were 9.21% and 8.19%, respectively. The converted star-8QAM signal exhibited a 0.6 dB power penalty over the input standard-8QAM signal at the HD-FEC level for the same input OSNR. For the ideal standard-8QAM signal with BTB transmission, the corresponding receiver OSNR is 21.3 dB. the converted star-8QAM signal obtains OSNR penalty of 1.4 dB. As shown in Fig. 9, the converted star-8QAM accumulated a significant amount of nonlinear phase noise from SPM and XPM. The higher power outer ring constellation points were particularly vulnerable. The phase offset of 45° between the inner and the outer rings of the input standard-shaped 8QAM signal can be eliminated by the pump assisted NOLM. Although the converted star-8QAM signals had worse BER performance, regardless of the input type, this format still offers better laser linewidth tolerance [53].

The converted star-8QAM can also be considered as a combination of QPSK signals with two rings. The amplitude shift keying (ASK) part of the star-8QAM obtained can be received using direct detection (DD) [54]. Moreover, as a hierarchically modulated optical signal, the ASK part can be sent to a traditional passive optical network (PON) and the QPSK part can be utilized in an advanced PON with digital signal processing (DSP) [55].

Since the fact that GCS is often achieved by changing the signal constellations distribution, this all-optical format inter-conversion of square-, standard- and star-8QAM signals can be viewed as GCS in the amplitude and the phase distributions. Deploying all-optical format interconversion configuration at the optical gateway is beneficial to the all-optical interconnection of homogeneous and heterogeneous optical networks by using different optical modulation formats. The pump assisted NOLM approach offers a general-purpose conversion method to achieve this.

Fig. 13 shows the conversion of 25 dB OSNR 10 GBaud square-8QAM into QPSK using the pump assisted NOLM. The amplitude and phase differences between the inner and the outer rings of the square-8QAM signal can be eliminated simultaneously. To the best of our knowledge, this is the first reported format conversion from square-8QAM to QPSK. Most existing schemes have only demonstrated format conversion from standard- and star-8QAM to QPSK [3], [9], [21], [56]. The PTF and the RPS of the format conversion from square-8QAM to QPSK are shown in Fig. 14 using a 21.8 dBm pump. When the input square-8QAM signal had an average power of 24 dBm, the corresponding output powers of the inner and the outer rings in the converted QPSK signal were 13.09 dBm and 14.29 dBm, respectively. There was a thus power gap of 1.2 dB between the inner and the outer rings power in the converted QPSK signal, reduced from the 3 dB gap between the inner and the outer rings of the input square-8QAM signal. The phase offset between adjacent input square-8QAM constellation points at the inner and the outer

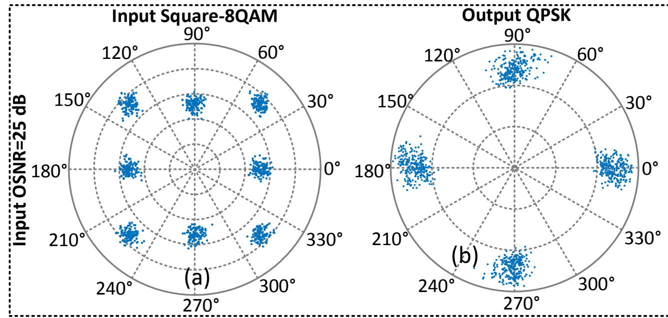

Fig. 13. Constellations of (a) the input 30 Gbit/s square-shaped 8QAM signal, (b) converted QPSK signal.

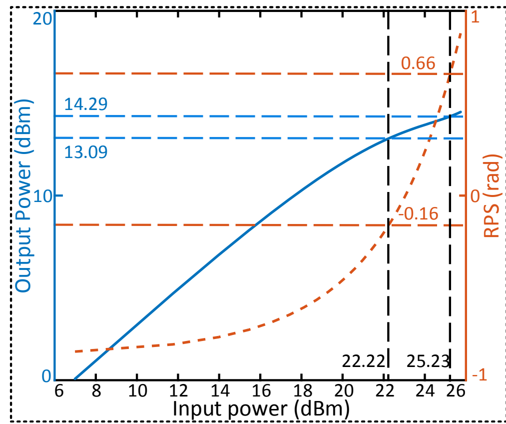

Fig. 14. PTF and RPS versus the input power for the format conversion from the 30Gbit/s square-shaped 8QAM signal to the QPSK signal.

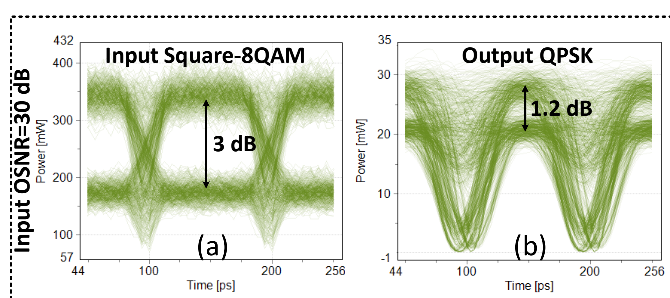

Fig. 15. Eye diagrams of (a) the input 30 Gbit/s square-shaped 8QAM signal, (b) converted QPSK signal.

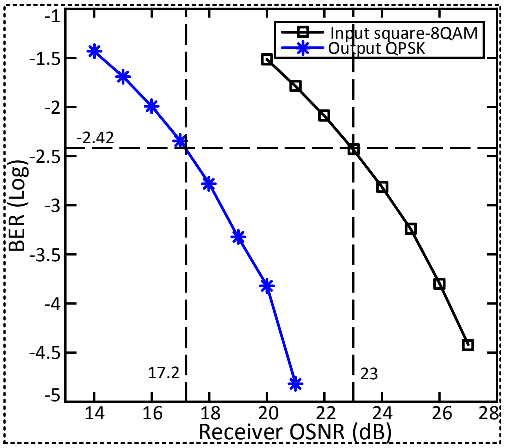

Fig. 16. BER versus receiver OSNR for the format conversion of square-shaped 8QAM to QPSK with the input OSNR of 25 dB.

rings can also be mitigated. For example, the output RPSs for the inner and the outer rings in the input square-8QAM were -0.16 rad and 0.66 rad, respectively. Moreover, the relative nonlinear phase difference was circa 47.17°, which was within 5% of the ideal value of 45°. Thus, the output signal was QPSK, albeit with the amplitude difference noted above. This can also be observed from the eye diagrams of square-8QAM and QPSK with a 30 dB OSNR input, shown in Fig. 15. The 3 dB square-8QAM power interval between the inner and the outer rings was reduced to 1.2 dB, which may be observed to be consistent with Fig. 14 in the QPSK signal simulation (Fig. 15(b)).

Fig. 16 shows the BER performance of the converted QPSK and the input square-8QAM, obtained from evaluating 2^{17}, 25 dB OSNR symbols. The converted signals offer a 5.8 dB receiver OSNR advantage at the HD-FEC limit resulting from the larger Euclidean distances between adjacent constellation points. Therefore, the pump assisted NOLM can be deployed at the optical gateway to obtain QPSK by amplitude and phase erasure of the square-8QAM signal.

IV. Conclusion

In this paper, a configurable all-optical format interconversion scheme of square-, standard- and star-shaped 8QAM signals based on a pump assisted NOLM is proposed and numerically simulated for the first time to our knowledge. Input square- and standard-8QAM signals can be converted into the star-8QAM and vice versa. Therefore, star-8QAM can be employed as the intermediate optical signal to realize all-optical format interconversion between the square- and standard-8QAM. When the input OSNR is set as 25 dB, the constellation and eye diagrams have been assessed to evaluate the optical format interconversion results intuitively. For converting square-8QAM to star-8QAM signal, the converted there was a 1.5 dB degradation in the receiver OSNR; for standard-8QAM to star-8QAM, the received OSNR degradation was just 0.6 dB. Finally, for conversion from star-8QAM to square- and standard-8QAM signals, the output signals had improvements of 4.3 dB and 5.4 dB respectively in their receiver OSNR values. Meanwhile, the proposed scheme was extended to realize conversion from the square-8QAM to QPSK, particularly at low OSNRs. The proposed scheme can be deployed in optical gateways to connect homogeneous and heterogeneous optical networks by dynamically selecting their optimal modulation formats. It also has the potential applied advantage in realizing the format conversion of wavelength division multiplexing (WDM) channels.

Acknowledgment

We acknowledge the reviewers and editors for their careful and constructive suggestions. Qiankun Li would like to thank his parents and friend Hao Zhang for happiness, company and support in the year 2020.

References

[1] W. Lautenschlaeger, N. Benzaoui, F. Buchali, L. Dembeck, R. Dischler, B. Franz, U. Gebhard, J. Milbrandt, Y. Pointurier, D. Roesener, L. Schmalen, and A. Leven, "Optical Ethernet—Flexible Optical Metro Networks," *J. Lightwave Technol.*, vol. 35, no. 12, pp. 2346–2357, Jun 2017. [Online]. Available: https://opg.optica.org/jlt/abstract.cfm?URI=jlt-35-12-2346

[2] J. S. Wey and J. Zhang, "Passive Optical Networks for 5G Transport: Technology and Standards," *J. Lightwave Technol.*, vol. 37, no. 12, pp. 2830–2837, Jun 2019. [Online]. Available: https://opg.optica.org/jlt/abstract.cfm?URI=jlt-37-12-2830

[3] Q. Li, X. Yang, and J. Yang, "All-Optical Aggregation and De-Aggregation Between 8QAM and BPSK Signal Based on Nonlinear Effects in HNLF," *J. Lightwave Technol.*, vol. 39, no. 17, pp. 5432–5438, Sep 2021. [Online]. Available: https://opg.optica.org/jlt/abstract.cfm?URI=jlt-39-17-5432

[4] X. Liu, "Enabling Optical Network Technologies for 5G and Beyond," *J. Lightwave Technol.*, vol. 40, no. 2, pp. 358–367, Jan 2022. [Online]. Available: https://opg.optica.org/jlt/abstract.cfm?URI=jlt-40-2-358

[5] "Cisco Annual Internet Report (2018-2023) White Paper," 2020. [Online]. Available: https://www.cisco.com/c/en/us/solutions/collateral/executive-perspectives/annual-internet-report/white-paper-c11-741490.html

[6] A. E. Willner, A. Fallahpour, F. Alishahi, Y. Cao, A. Mohajerin-Ariaei, A. Almaiman, P. Liao, K. Zou, A. N. Willner, and M. Tur, "All-Optical Signal Processing Techniques for Flexible Networks," *J. Lightwave Technol.*, vol. 37, no. 1, pp. 21–35, Jan 2019. [Online]. Available: https://opg.optica.org/jlt/abstract.cfm?URI=jlt-37-1-21

[7] Y. R. Zhou, J. Keens, and W. Wakim, "High Capacity Innovations Enabling Scalable Optical Transmission Networks," in *Optical Fiber Communication Conference (OFC) 2022*. Optica Publishing Group, 2022, p. W3C.3. [Online]. Available: https://opg.optica.org/abstract.cfm?URI=OFC-2022-W3C.3

[8] P. J. Winzer, "High-Spectral-Efficiency Optical Modulation Formats," *J. Lightwave Technol.*, vol. 30, no. 24, pp. 3824–3835, Dec 2012. [Online]. Available: https://opg.optica.org/jlt/abstract.cfm?URI=jlt-30-24-3824

[9] X. Zhou and J. Yu, "Multi-Level, Multi-Dimensional Coding for High-Speed and High-Spectral-Efficiency Optical Transmission," *J. Lightwave Technol.*, vol. 27, no. 16, pp. 3641–3653, Aug 2009. [Online]. Available: https://opg.optica.org/jlt/abstract.cfm?URI=jlt-27-16-3641

[10] X. Zhou, J. Yu, D. Qian, T. Wang, G. Zhang, and P. D. Magill, "High-Spectral-Efficiency 114-Gb/s Transmission Using PolMux-RZ-8PSK Modulation Format and Single-Ended Digital Coherent Detection Technique," *J. Lightwave Technol.*, vol. 27, no. 3, pp. 146–152, Feb 2009. [Online]. Available: https://opg.optica.org/jlt/abstract.cfm?URI=jlt-27-3-146

[11] Y. Lu, F. Liu, M. Qiu, and Y. Su, "All-optical format conversions from NRZ to BPSK and QPSK based on nonlinear responses in silicon microring resonators," *Opt. Express*, vol. 15, no. 21, pp. 14 275–14 282, Oct 2007. [Online]. Available: https://opg.optica.org/oe/abstract.cfm?URI=oe-15-21-14275

[12] R. Rios-Mller, J. Renaudier, P. Tran, and G. Charlet, "Experimental comparison of two 8-QAM constellations at 200 Gb/s over ultra long-haul transmission link," in *2014 The European Conference on Optical Communication (ECOC)*, 2014, pp. 1–3.

[13] P. J. Winzer, A. H. Gnauck, C. R. Doerr, M. Magarini, and L. L. Buhl, "Spectrally Efficient Long-Haul Optical Networking Using 112-Gb/s Polarization-Multiplexed 16-QAM," *J. Lightwave Technol.*, vol. 28, no. 4, pp. 547–556, Feb 2010. [Online]. Available: https://opg.optica.org/jlt/abstract.cfm?URI=jlt-28-4-547

[14] J. M. D. Mendinueta, S. Shinada, Y. Hirota, H. Furukawa, and N. Wada, "High-Capacity Super-Channel-Enabled Multi-Core Fiber Optical Switching System for Converged Inter/Intra Data Center and Edge Optical Networks," *IEEE Journal of Selected Topics in Quantum Electronics*, vol. 26, no. 4, pp. 1–13, 2020.

[15] N. Sotiropoulos, T. Koonen, and H. de Waardt, "Advanced Differential Modulation Formats for OpticalAccess Networks," *J. Lightwave Technol.*, vol. 31, no. 17, pp. 2829–2843, Sep 2013. [Online]. Available: https://opg.optica.org/jlt/abstract.cfm?URI=jlt-31-17-2829

[16] Y. Lu, F. Liu, M. Qiu, and Y. Su, "All-optical format conversions from NRZ to BPSK and QPSK based on nonlinear responses in silicon microring resonators," *Opt. Express*, vol. 15, no. 21, pp. 14 275–14 282, Oct 2007. [Online]. Available: https://opg.optica.org/oe/abstract.cfm?URI=oe-15-21-14275

[17] A. Fallahpour, F. Alishahi, K. Zou, Y. Cao, A. Almaiman, A. Kordts, M. Karpov, M. H. P. Pfeiffer, K. Manukyan, H. Zhou, P. Liao, C. Liu, M. Tur, T. J. Kippenberg, and A. E. Willner, "Demonstration of Tunable Optical Aggregation of QPSK to 16-QAM Over Optically Generated Nyquist Pulse Trains Using Nonlinear Wave Mixing and a Kerr Frequency Comb," *J. Lightwave Technol.*, vol. 38, no. 2, pp. 359–365, Jan 2020. [Online]. Available: https://opg.optica.org/jlt/abstract.cfm?URI=jlt-38-2-359

[18] Y. Ding, H. Wang, and J. Yuefeng, "Experimental demonstration of all-optical aggregation and de-aggregation for a QPSK signal in an elastic optical network," *Opt. Express*, vol. 30, no. 5, pp. 6456–6468, Feb 2022. [Online]. Available: https://opg.optica.org/oe/abstract.cfm?URI=oe-30-5-6456

[19] Q. Li, X. Yang, H. Wen, Q. Xu, J. Yang, and H. Yang, "All-Optical Format Conversion for Star-8QAM Signals Based on Nonlinear Effects in Elastic Optical Networks," *J. Lightwave Technol.*, vol. 41, no. 2, pp. 440–450, Jan 2023. [Online]. Available: https://opg.optica.org/jlt/abstract.cfm?URI=jlt-41-2-440

[20] A. Misra, S. Preussler, K. Singh, J. Meier, and T. Schneider, "Modulation Format Aggregation of Nyquist channels by Spectral Superposition with Electro-Optic Modulators," in *Optical Fiber Communication Conference (OFC) 2022*. Optica Publishing Group, 2022, p. W2A.28. [Online]. Available: https://opg.optica.org/abstract.cfm?URI=OFC-2022-W2A.28

[21] H. Liu, H. Wang, and Y. Ji, "Simultaneous All-Optical Channel Aggregation and De-Aggregation for 8QAM Signal in Elastic Optical Networking," *IEEE Photonics Journal*, vol. 11, no. 1, pp. 1–8, 2019.

[22] M. Ziyadi, A. Mohajerin-Ariaei, A. Almaiman, Y. Cao, M. R. Chitgarha, L. Paraschis, M. Tur, C. Langrock, M. M. Fejer, J. D. Touch, and A. E. Willner, "Optical channel de-aggregation of quadrature-phase-shift-keying and eight-phase-shift-keying data using mapping onto constellation axes," *Opt. Lett.*, vol. 40, no. 21, pp. 4899–4902, Nov 2015. [Online]. Available: https://opg.optica.org/ol/abstract.cfm?URI=ol-40-21-4899

[23] A. Fallahpour, A. Mohajerin-Ariaei, A. Almaiman, Y. Cao, F. Alishahi, C. Bao, P. Liao, M. Ziyadi, B. Shamee, D. Starodubov, M. Tur, C. Langrock, M. M. Fejer, J. Touch, and A. E. Willner, "Demonstration of 30Gbit/s QPSK-to-PAM4 Data-Format and Wavelength Conversion to Enable All-Optical Gateway from Long-haul to Datacenter," in *Optical Fiber Communication Conference*. Optica Publishing Group, 2018, p. W2A.22. [Online]. Available: https://opg.optica.org/abstract.cfm?URI=OFC-2018-W2A.22

[24] T. Kodama, T. Koike-Akino, K. Kojima, and K. Parsons, "DNN-assisted phase distance tuned PSK modulation for PAM4-to-QPSK format conversion gateway node," *Opt. Express*, vol. 30, no. 7, pp. 10 866–10 876, Mar 2022. [Online]. Available: https://opg.optica.org/oe/abstract.cfm?URI=oe-30-7-10866

[25] H. Wang, G. Li, and Y. Ji, "Phase and amplitude regeneration of a rectangular 8-QAM in a phase-sensitive amplifier with low-order harmonics," *Appl. Opt.*, vol. 56, no. 3, pp. 506–509, Jan 2017. [Online]. Available: https://opg.optica.org/ao/abstract.cfm?URI=ao-56-3-506

[26] Q. Li, J. Yang, X. Yang, Q. Xu, H. Zhang, Y. Liang, and H. Yang, "All-Optical Format Conversion of 2-Dimensional MQAM to MPSK Based on Nonlinear Mach-Zehnder Interferometer With Wavelength Preservation," *J. Lightwave Technol.*, vol. 40, no. 22, pp. 7246–7253, Nov 2022. [Online]. Available: https://opg.optica.org/jlt/abstract.cfm?URI=jlt-40-22-7246

[27] P. Leoni, S. Calabro, and B. Lankl, "Constellation Expansion for Differentially Encoded 100G Transmission," *Photonics Technology Letters, IEEE*, vol. 26, pp. 1142–1145, 06 2014.

[28] J. Yu and X. Zhou, "Ultra-High-Capacity DWDM transmission system for 100G and beyond," *IEEE Communications Magazine*, vol. 48, no. 3, pp. S56–S64, 2010.

[29] D. Qian, M.-F. Huang, S. Zhang, P. N. Ji, Y. Shao, F. Yaman, E. Mateo, T. Wang, Y. Inada, T. Ogata, and Y. Aoki, "Transmission of 115×100G PDM-8QAM-OFDM Channels with 4bits/s/Hz Spectral Efficiency over 10,181km," in *37th European Conference and Exposition on Optical Communications*. Optica Publishing Group, 2011, p. Th.13.K.3. [Online]. Available: https://opg.optica.org/abstract.cfm?URI=ECOC-2011-Th.13.K.3

[30] J. Zhang, J. Yu, and H.-C. Chien, "Linear and Nonlinear Compensation for 8-QAM SC-400G Long-Haul Transmission Systems," *J. Lightwave Technol.*, vol. 36, no. 2, pp. 495–500, Jan 2018. [Online]. Available: https://opg.optica.org/jlt/abstract.cfm?URI=jlt-36-2-495

[31] M. Nölle, F. Frey, R. Elschner, C. Schmidt-Langhorst, A. Napoli, and C. Schubert, "Performance Comparison of Different 8QAM Constellations for the Use in Flexible Optical Networks," in *Optical Fiber Communication Conference*. Optica Publishing Group, 2014, p. W3B.2. [Online]. Available: https://opg.optica.org/abstract.cfm?URI=OFC-2014-W3B.2

[32] L. Nadal, J. M. Fbrega, J. Vılchez, and M. Svaluto Moreolo, "Experimental Analysis of 8-QAM Constellations for Adaptive Optical OFDM Systems," *IEEE Photonics Technology Letters*, vol. 28, no. 4, pp. 445–448, 2016.

[33] P. Zou, Y. Liu, F. Wang, and N. Chi, "Mitigating Nonlinearity Characteristics of Gray-Coding Square 8QAM in Underwater VLC system," in *Asia Communications and Photonics Conference (ACP) 2018*. Optica Publishing Group, 2018, p. Su4D.3. [Online]. Available: https://opg.optica.org/abstract.cfm?URI=ACPC-2018-Su4D.3

[34] P. Song, Z. Hu, and C.-K. Chan, "Performance Comparison of Different 8-QAM Constellations Used in SEFDM systems," in *2021 Opto-Electronics and Communications Conference (OECC)*, 2021, pp. 1–3.

[35] Q. Wang, Z. Quan, S. Bi, C. Yu, and P.-Y. Kam, "Generalized Mutual Information Analysis for BICM-8QAM With Residual Phase Noise," *IEEE Communications Letters*, vol. 25, no. 12, pp. 3819–3823, 2021.

[36] Y. Wan, B. Liu, J. Ren, R. Ullah, Y. Mao, S. Zhu, S. Chen, X. Wu, F. Wang, T. Sun, Y. Wu, and L. Zhao, "Performance-Enhanced Optical Non-Orthogonal Multiple Access Enabled by Orthogonal Chirp Division Multiplexing," *J. Lightwave Technol.*, vol. 40, no. 16, pp. 5440–5449, Aug 2022. [Online]. Available: https://opg.optica.org/jlt/abstract.cfm?URI=jlt-40-16-5440

[37] X. Pan, Y. Liu, and L. Guo, "Asymmetric constellation transmission for a coherent free-space optical system with spatial diversity," *Opt. Lett.*, vol. 46, no. 20, pp. 5157–5160, Oct 2021. [Online]. Available: https://opg.optica.org/ol/abstract.cfm?URI=ol-46-20-5157

[38] B. Stiller, G. Onishchukov, B. Schmauss, and G. Leuchs, "Phase regeneration of a star-8QAM signal in a phase-sensitive amplifier with conjugated pumps," *Opt. Express*, vol. 22, no. 1, pp. 1028–1035, Jan 2014. [Online]. Available: https://opg.optica.org/oe/abstract.cfm?URI=oe-22-1-1028

[39] N. J. Doran and D. Wood, "Nonlinear-optical loop mirror," *Opt. Lett.*, vol. 13, no. 1, pp. 56–58, Jan 1988. [Online]. Available: https://opg.optica.org/ol/abstract.cfm?URI=ol-13-1-56

[40] A. Bogoni, P. Ghelfi, M. Scaffardi, and L. Poti, "All-optical regeneration and demultiplexing for 160-gb/s transmission systems using a NOLM-based three-stage scheme," *IEEE Journal of Selected Topics in Quantum Electronics*, vol. 10, no. 1, pp. 192–196, 2004.

[41] G. Huang, Y. Miyoshi, A. Maruta, Y. Yoshida, and K.-I. Kitayama, "All-Optical OOK to 16-QAM Modulation Format Conversion Employing Nonlinear Optical Loop Mirror," *J. Lightwave Technol.*, vol. 30, no. 9, pp. 1342–1350, May 2012. [Online]. Available: https://opg.optica.org/jlt/abstract.cfm?URI=jlt-30-9-1342

[42] C. Guo, M. Vasilyev, and T. I. Lakoba, "Amplitude regeneration and phase noise suppression of an 8-PSK signal by an attenuation-imbalanced NOLM," in *Conference on Lasers and Electro-Optics*. Optica Publishing Group, 2022, p. STh5M.6.

[43] Z. Wang, I. Glesk, and L. R. Chen, "An integrated nonlinear optical loop mirror in silicon photonics for all-optical signal processing," *APL Photonics*, vol. 3, no. 2, p. 026102, 2018. [Online]. Available: https://doi.org/10.1063/1.5013618

[44] Z. Jia, J. Yu, G. Ellinas, and G.-K. Chang, "Key Enabling Technologies for Optical–Wireless Networks: Optical Millimeter-Wave Generation, Wavelength Reuse, and Architecture," *J. Lightwave Technol.*, vol. 25, no. 11, pp. 3452–3471, Nov 2007. [Online]. Available: https://opg.optica.org/jlt/abstract.cfm?URI=jlt-25-11-3452

[45] Y. Miyoshi, S. Takagi, S. Namiki, and K.-I. Kitayama, "Multiperiod PM-NOLM With Dynamic Counter-Propagating Effects Compensation for 5-Bit All-Optical Analog-to-Digital Conversion and Its Performance Evaluations," *J. Lightwave Technol.*, vol. 28, no. 4, pp. 415–422, Feb 2010. [Online]. Available: https://opg.optica.org/jlt/abstract.cfm?URI=jlt-28-4-415

[46] A. Bogoni, M. Scaffardi, P. Ghelfi, and L. Poti, "Nonlinear optical loop mirrors: investigation solution and experimental validation for undesirable counterpropagating effects in all-optical signal processing," *IEEE Journal of Selected Topics in Quantum Electronics*, vol. 10, no. 5, pp. 1115–1123, 2004.

[47] F. Wen, B. Wu, K. Qiu, and S. Sygletos, "Conjugate nonlinear-optical loop mirror (Conj-NOLM)-based phase-preserving multilevel amplitude regenerator," *Opt. Express*, vol. 27, no. 14, pp. 19 940–19 949, Jul 2019. [Online]. Available: https://opg.optica.org/oe/abstract.cfm?URI=oe-27-14-19940

[48] Q. Li, H. Lin, and Q. Xu, "Analytical Solution of All-Optical Format Conversion Based on the XPM Effect," in *2022 Asia Communications and Photonics Conference (ACP)*, 2022, pp. 389–392. [Online]. Available: https://ieeexplore.ieee.org/document/10089000

[49] J. Hansryd, F. Dross, M. Westlund, P. A. Andrekson, and S. N. Knudsen, "Increase of the sbs threshold in a short highly nonlinear fiber by applying a temperature distribution," *J. Lightwave Technol.*, no. 11, p. 1691.

[50] C. Lundstrom, R. Malik, L. Gruner-Nielsen, B. Corcoran, S. L. I. Olsson, M. Karlsson, and P. A. Andrekson, "Fiber Optic Parametric Amplifier With 10-dB Net Gain Without Pump Dithering," *IEEE Photonics Technology Letters*, vol. 25, no. 3, pp. 234 – 237, 2013.

[51] B. Guo, F. Wen, B. Wu, and K. Qiu, "All-optical multi-level amplitude regenerator in a polarization-effect optimized nonlinear-optical loop mirror (PE-NOLM) configuration," *Opt. Express*, vol. 31, no. 8, pp. 12 725–12 738, Apr 2023. [Online]. Available: https://opg.optica.org/oe/abstract.cfm?URI=oe-31-8-12725

[52] T. Roethlingshoefer, T. Richter, C. Schubert, G. Onishchukov, B. Schmauss, and G. Leuchs, "All-optical phase-preserving multilevel amplitude regeneration," *Opt. Express*, vol. 22, no. 22, pp. 27 077–27 085, Nov 2014. [Online]. Available: https://opg.optica.org/oe/abstract.cfm?URI=oe-22-22-27077

[53] H. Zhang, P.-Y. Kam, and C. Yu, "Performance analysis of coherent optical 8-star QAM systems using decision-aided maximum likelihood phase estimation," *Opt. Express*, vol. 20, no. 8, pp. 9302–9311, Apr 2012. [Online]. Available: https://opg.optica.org/oe/abstract.cfm?URI=oe-20-8-9302

[54] G.-W. Lu and T. Miyazaki, "Experimental Demonstration of RZ-8-APSK Generation Through Optical Amplitude and Phase Multiplexing," *IEEE Photonics Technology Letters*, vol. 20, no. 23, pp. 1995–1997, 2008.

[55] N. Iiyama, J. ichi Kani, J. Terada, and N. Yoshimoto, "Feasibility Study on a Scheme for Coexistence of DSP-Based PON and 10-Gbps/λ PON Using Hierarchical Star QAM Format," *J. Lightwave Technol.*, vol. 31, no. 18, pp. 3085–3092, Sep 2013. [Online]. Available: https://opg.optica.org/jlt/abstract.cfm?URI=jlt-31-18-3085

[56] H. Kishikawa, M. Uetai, and N. Goto, "All-Optical Modulation Format Conversion Between OOK, QPSK, and 8QAM," *J. Lightwave Technol.*, vol. 37, no. 16, pp. 3925–3931, Aug 2019. [Online]. Available: https://opg.optica.org/jlt/abstract.cfm?URI=jlt-37-16-3925